SCIENCE CHINA Materials LETTERS

mater.scichina.com link.springer.com

Published online 15 January 2021 | https://doi.org/10.1007/s40843-020-1589-7
Sci China Mater 2021, 64(6): 1563–1569

Ultra-stable 2D cuprofullerene imidazolate polymer as a high-performance visible-light photodetector

Shun-Ze Zhan[1*], Jing-Hong Li[1], Yanzhou Li[3,4], Gang Xu[3], Deng-Feng Luo[1], Li Dang[1] and Dan Li[2*]

Since the discovery of C_{60} [1], considerable efforts have been made to explore the potential applications of fullerene-based materials in photoelectronic devices [2–9]. Such materials show highly efficient charge carrier generation and separation upon light illumination due to their spherical polyene structure and high electron affinity [10]. Many C_{60}-based composite materials, including C_{60}-embedded metal-organic frameworks (MOFs) [11,12], C_{60}-doped polymers [2], organic C_{60} derivatives [7,13–15], and C_{60}-anchored perovskite films [16], show advantageous photoelectronic performances by virtue of highly efficient photogenerated donor-acceptor charge transfer [17–19]. However, only a small number of these materials exhibit precise crystal structures, which hampers the evaluation of their structure-function relationships.

Pristine C_{60} crystalline nanostructures have been reported to show high photoelectronic performance due to their highly oriented C_{60} alignment and interfullerene distances [3–6,20,21]. However, the crystalline metastability and rotational disorder of C_{60} spheres in such nanomaterials, which occur due to a lack of strong bonding interactions between C_{60} molecules [22], may seriously affect their photoelectronic functions and limit their application [4,5]. Consequently, the fabrication of highly stable crystalline materials with highly oriented C_{60} alignment is crucial to enable their practical application as photoelectronic devices.

Thirty pairs of π-electrons in a spherical C_{60} molecule provide abundant coordination sites for the binding of multiple metals in η^2-fashions, forming exohedral metallofullerene clusters [23,24] and polymers [10,25–29]. Compared with these C_{60} nanomaterials, exohedral metallofullerene polymers exhibit higher crystalline stability for the stronger coordination bonds than in non-bonding interactions. Furthermore, the effective overlaps of pπ-dπ orbitals between C_{60} and metals facilitate strong electronic coupling between both components [10,30]. These advantages significantly enhance the functionality of these exohedral metallofullerene polymers. However, few metallofullerene polymers, for example, one dimensional (1D) $\{[Ni(Me_3P)_2](\mu_2\text{-}\eta^2,\eta^2\text{-}C_{60})\}_\infty$ [26], exhibit a crystalline structure. Pd_nC_{60}/Pt_nC_{60} polymeric materials have been shown to have conductive properties [10,25], but were prepared as amorphous polymers [10,31,32]. At present, it remains a great challenge to prepare crystalline exohedral metallofullerene polymers [10,25,33], let alone to explore their photoelectrical functions.

Most crystalline exohedral metallofullerenes are prepared according to the traditional solution-based synthesis [10]. Recently, solvothermal synthesis was used to prepare metallofullerenes and a series of high nuclear cuprofullerenes were afforded [23,24]. The direct complexation of Cu(I) atoms increases their absorption efficiency for visible light relative to pristine C_{60} [23,24], thus providing an advantageous strategy for the preparation of photoelectronic metallofullerene materials with responses to visible light.

On the basis of our previous work concerning disk-type nano-Saturn complexes $[Cu_{10}(Mim)_{10}]\supset C_{60}/C_{70}$ (Mim = 2-methylimidazolate) [34], we herein report a 2D sheet-like cuprofullerene imidazolate polymer $[(CuIm)_2C_{60}]_n$

[1] Department of Chemistry and Key Laboratory for Preparation and Application of Ordered Structural Materials of Guangdong Province, Shantou University, Shantou 515063, China
[2] College of Chemistry and Materials Science, and Guangdong Provincial Key Laboratory of Functional Supramolecular Coordination Materials and Applications, Jinan University, Guangzhou 510632, China
[3] State Key Laboratory of Structural Chemistry, Fujian Institute of Research on the Structure of Matter, Chinese Academy of Sciences (CAS), Fuzhou 350002, China
[4] College of Chemistry and Chemical Engineering, Henan University, Kaifeng 475004, China
* Corresponding authors (emails: szzhan@stu.edu.cn (Zhan SZ); danli@jnu.edu.cn (Li D))

 © Science China Press and Springer-Verlag GmbH Germany, part of Springer Nature 2021

(Im = imidazolate). This material shows both highly ordered C_{60} alignment and extraordinary chemical stability and high performance for a photodetector upon visible light irradiation. The complex was prepared with a yield of 79.8% under solvothermal conditions (Scheme 1a and Figs S1–S3). It crystallized in the $P2_1/c$ space group (Table S1), thereby giving a 2D sheet structure (Scheme 1b). The 1D chainlike Cu(I)-imidazolate exhibits a 2_1 screw (Fig. S4a), and two opposite chiral $(CuIm)_n$ chains are cross-linked by linear μ_2-η^2:η^2-C_{60} from two opposite C=C bonds (Figs S3, S4a) to form a 2D sheet in which C_{60} exhibits the same coordination as the 1D $\{[Ni(Me_3P)_2](\mu_2\text{-}\eta^2\text{:}\eta^2\text{-}C_{60})\}_\infty$ polymer [26]. Each Cu(I) shows 3-coordination geometry bound by two N atoms and one C=C bond. The Cu–N (1.957(2) and 1.966(2) Å) and Cu −C (2.024(3) and 2.042(2) Å) distances are slightly longer than those of other Cu(I) imidazolate [35] and cuprofullerene/Cu(I)-olefin complexes [23,36], indicating the bulky crowd effects of C_{60} moieties. The coordinated C=C shows a slightly larger length (1.440(6) Å) than other uncoordinated C=C (1.380–1.400 Å), similar to that of previously reported cuprofullerenes [23].

As reported for Cu(I)-pyrazolate complexes [37], the linear Cu(I) centers in $(CuIm)_n$ chains provide potential vacant sites for further coordination by C=C. However, $[(CuIm)_2C_{60}]_n$ shows a distinctly different structure from previously reported nano-Saturn $[Cu_{10}(Mim)_{10}]\supset C_{60}$ [34]. The interaction differences between fullerene moieties and either $(CuIm)_n$ chains or $Cu_{10}(Mim)_{10}$ rings demonstrate the substituent effects of methyl, which provides sufficient C−H for C−H···π interactions between the Mim and fullerene moieties to induce the formation of closed $Cu_{10}(Mim)_{10}$ macrocycles and stabilize the nano-Saturn system [34], and also a bulky crowd capable of preventing C_{60} from coordinating on Cu(I) atoms.

In each sheet, C_{60} spheres are arranged parallel to the [201] crystallographic plane (Fig. 1a and Fig. S4a), and the shortest $C_{60}\cdots C_{60}$ center distance (9.717(2) Å) exists

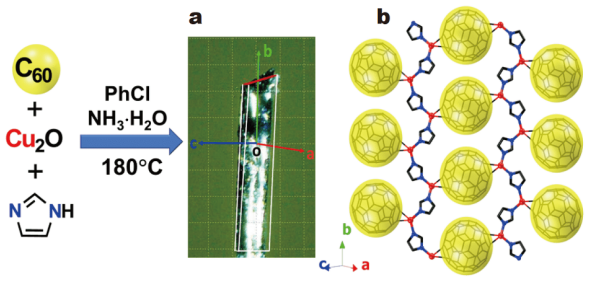

Scheme 1 Synthesis of the cuprofullerene imidazolate polymer, showing the crystal image (a) and sheet-like structure (b).

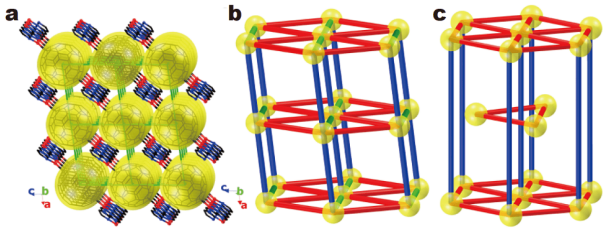

Figure 1 Packing structures (a) showing the inclined hexagonal frontal packed (*i-hfp*) C_{60} moieties (b) in the complex. The *hcp* C_{60} crystalline structure is shown in (c) as a comparison.

along the $(CuIm)_n$ chains (Fig. S4a). These sheets are stacked together through intersheet convex-concave π···π interactions (Im···C_{60} and $C_{60}\cdots C_{60}$). The shortest distances between the center of Im and the adjacent atom of C_{60} are 3.239(2) and 3.325(6) Å (Fig. S5), respectively, and the corresponding shortest C···C distances between C_{60} moieties are 3.109(1) and 2.845(8) Å. Accordingly, these C_{60} moieties are arranged in an inclined hexagonal frontal packed (*i-hfp*) formation (Fig. 1a, b and Fig. S6). Each C_{60} molecule is in contact with eight other C_{60} molecules close to the $C_{60}\cdots C_{60}$ center distances of 9.929(1) Å (red), 9.822(1) Å (blue), and 9.717(1) Å (green), respectively (Fig. 1b). These distances are similar to those in a pristine crystalline C_{60} solid in a face-centered cubic (*fcc*) or hexagonal closed packed (*hcp*) crystalline structures [5] (Fig. 1c), possibly implying that photoelectronic functions are conserved in the pristine crystalline C_{60} solid.

The crystalline sample shows high thermal stability, with the thermal gravity analysis (TGA) demonstrating that it begins to lose weight above 600°C (Fig. 2a and Fig. S7). However, temperature-dependent powder X-ray diffraction (TD-PXRD) patterns exhibit irreversible phase transformations above 325°C (Fig. 2b and Fig. S8), further evidenced by a strong endothermic peak at approximately 325°C detected by the first cyclic differential scanning calorimeter (DSC) analysis (red line in Fig. 2a), which disappears in the second cycle (black dotted line in Fig. 2a and Fig. S9). Unfortunately, determination of the crystal structure of the heated crystal sample above 325°C was not possible due to the poor resulting single crystal XRD patterns.

The complex thus shows extraordinary chemical stability in acid/base and common solvents. When soaked in HCl/NaOH solutions with pH values ranging from 1.0 to 12.0 and even in 25% $NH_3{\cdot}H_2O$, or when soaked in thirteen common organic solvents for one week at room temperature (Fig. S10), the solid samples show highly consistent PXRD patterns (Fig. S11). It is believed that

© Science China Press and Springer-Verlag GmbH Germany, part of Springer Nature 2021

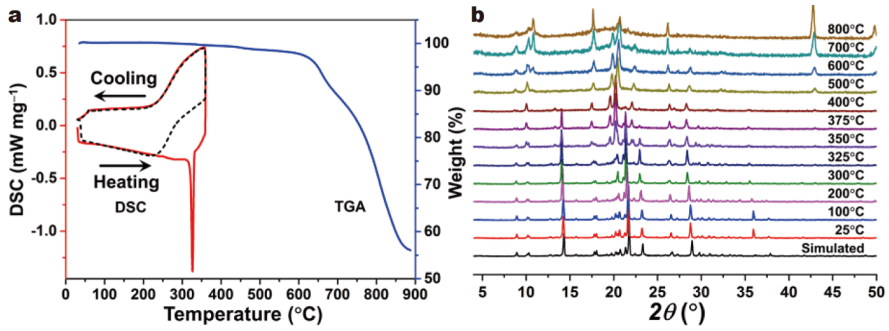

Figure 2 DSC (red and black dotted lines in a), TGA curves (blue line in a) and TD-PXRD patterns (b) of the as-prepared complex.

this chemical stability is closely related to synergistic convex-concave interactions between the constituent 2D sheets, which greatly increase the contact area between the sheets and protect $(CuIm)_n$ chains from being attacked by other molecules.

Similar to the reported cuprofullerene complexes [23], the complex shows a strong light absorption across the whole ultraviolet-visible (UV-Vis) and near infrared (NIR) region (Fig. 3a). Tauc plot demonstrates that the optical bandgap may be as narrow as 1.12 eV (Fig. 3b). Density functional theory calculations reveal an indirect bandgap structure [38] with a bandgap of 1.05 eV (Fig. 3c). Cyclic voltammetry measurements show an energy gap of 0.92 eV (Fig. S12). Compared with the direct bandgap (1.267 eV) of *fcc*-C_{60} crystals (Fig. S13), the indirect and much smaller bandgap of the complex implies a potential fast and highly efficient charge separation and a strongly suppressed charge carrier recombination [39], which is believed to be related to the complexation of Cu(I) atoms associated with C_{60} molecules. Density of states (DOS) demonstrate that both the valence band maximum at the Z point and the conduction band

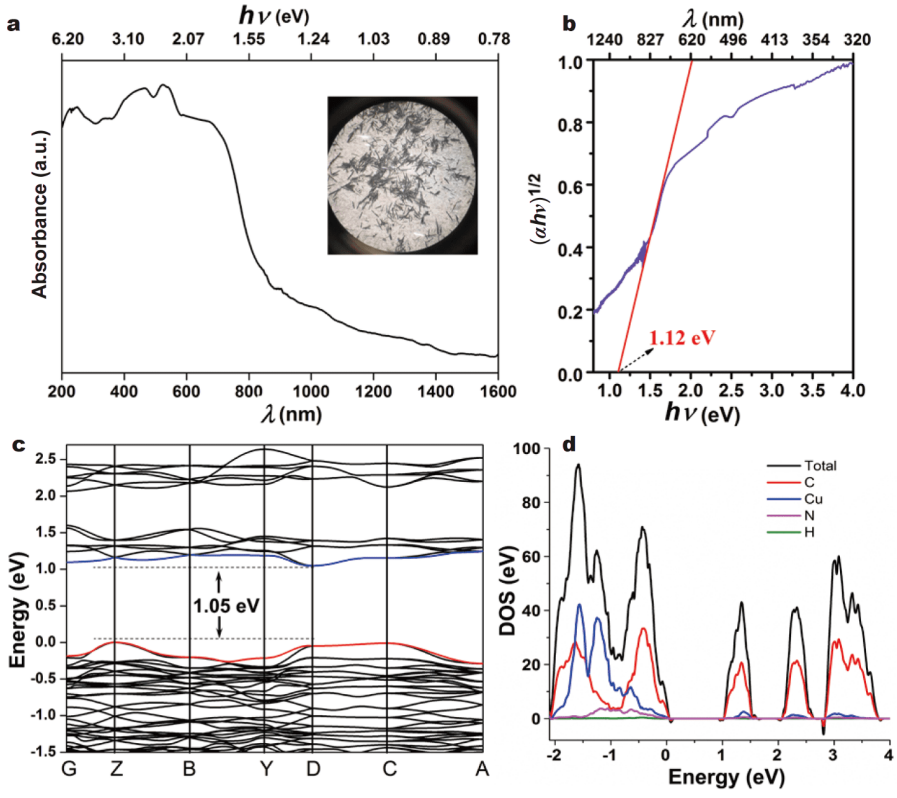

Figure 3 (a) UV-Vis spectrum; (b) Tauc plot; (c) calculated band structures; (d) DOS of the complex.

 © Science China Press and Springer-Verlag GmbH Germany, part of Springer Nature 2021

minimum at the D point are dominantly constructed by the 2p-orbitals of C atoms from C_{60} with a very small contribution from the 3d-orbitals of Cu(I) atoms (Fig. 3c, d and Fig. S14). These results imply that the 2D cuprofullerene complex inherits the photoelectric characters of these crystalline C_{60} nanomaterials [2–6,8]. Consequently, its photoelectronic performance as a photodetector was investigated.

The electrical conductivity of the powder pellet was measured as 7.69×10^{-10} S cm^{-1} (Fig. S15), similar to that of pure C_{60} single crystals [40,41], but much higher than that of the C_{60} solid film [42], indicating a near-insulating material without light illumination at room temperature.

Photoconductivity denotes the combined effects of optical and electronic properties [3,5]. To construct a photodetector device, a one-column single crystal of cuprofullerene polymer was placed on a glass substrate. The ends of the crystal were painted with a conductive silver paste spaced 200 μm across silver electrodes in order to secure a conductive pathway to the patterned electrodes (Fig. 4a and Fig. S16). Crystallographic indexing demonstrated that the longest direction of the column crystal was aligned with the crystallographic *b* axis, i.e., the extension direction of the $[Cu(Im)]_n$ chains (Scheme 1).

Under a 5.0 V bias voltage, the device shows significant photocurrent increase (on/off ratio) by approximately two orders of magnitude higher under incident white light illumination than dark current (Fig. S17). The bias-dependent R_λ measurement shows that R_λ increases quickly below 2.0 V before flattening out at around 5 V when irradiated with 500 nm radiation (Fig. S18). Therefore, a 5.0 V bias voltage was used to evaluate the performance of the device. Wavelength-dependent photocurrent measurements between 250 and 750 nm reveal a maximum detector current responsivity (R_λ) of 11.6 A W^{-1} under the optimized incident light conditions of 500 nm (Fig. 4a and Figs S19–S21), which is in agreement with UV-Vis absorption. For $[(CuIm)_2C_{60}]_n$ materials, photons in the whole UV-Vis region effectively contribute to the photoconductive effect due to the small band gap (~1.12 eV) (Fig. 3b). Interestingly, the responsivity in the region between 400 and 600 nm is in agreement with the absorption intensity of the polymer (Fig. 3a). These observations demonstrate that intense absorption can capture more photons effectively to produce photoinduced carrier, resulting in a strong photocurrent and high photoelectric performance.

A quick response and complete recovery to the ground state happen upon incident light on/off across all UV and

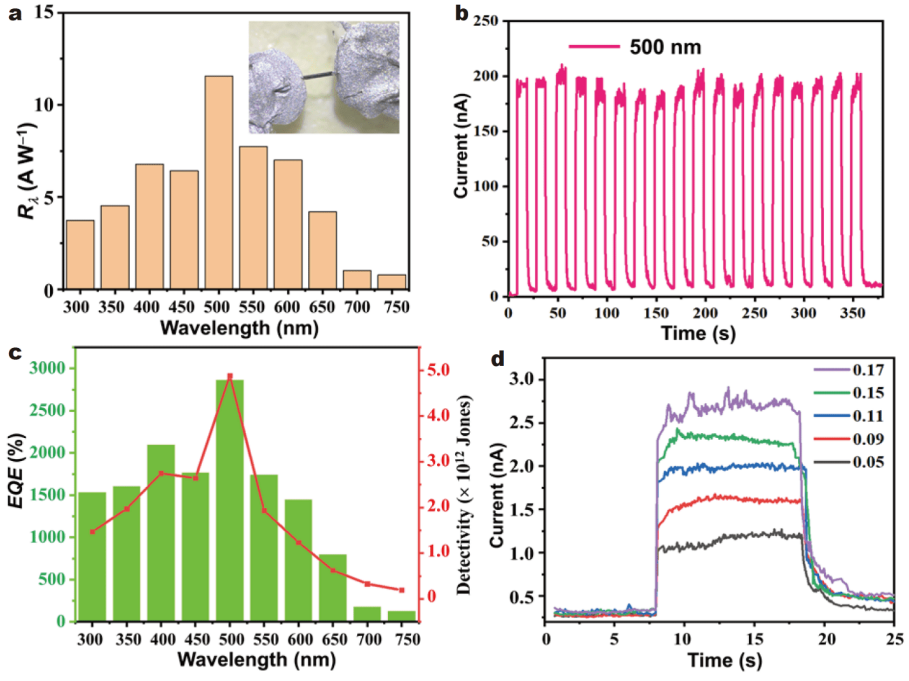

Figure 4 Photoelectrical measurements for the photodetector at a bias voltage of 5.0 V. (a, c) Calculated R_λ, EQE, and D^* at different wavelengths. (b) Periodic measurements of photocurrent under 500 nm light showing high photoelectrical stability. (d) *I*–*V* measurements and time sweep of the device under 500 nm illumination with different light power (mW cm^{-2}).

© Science China Press and Springer-Verlag GmbH Germany, part of Springer Nature 2021

Table 1 Summary of the photoelectric effects of the complex and reported pristine C_{60} materials[a]

Entry	λ (nm)	R_λ(mA W^{-1})	EQE (%)	D^* (Jones)	On/off ratio	Rise/decay time	θ	Reference
1	500	11.6×10^3	2866	4.88×10^{12}	100	0.3 s/1.0 s	0.77	This work
2	450–500	0.0213	\	1.7×10^7	\	50 μs/4 ms	0.94 1.25	[3]
3	400	2.5956×10^3	800	2.7×10^{12}	540	40 ms/8 ms	0.9	[5]
4	400	8.01	2.5	7.08×10^8	365	1.8 s/2.0 s	0.865	[4]
5	488	0.85	\	3.8×10^7	\	60 μs / \	\	[21]
6[b]	800	0.17×10^3	26	2.3×10^{13}	\	\	\	[2]

a) "\": not reported. b) PDDTT:$PC_{60}BM$ bulk heterojunction composites (PDDTT = poly(5,7-bis(4-decanyl-2-thienyl)-thieno(3,4-*b*)diathiazole-thiophene-2,5; $PC_{60}BM$ = (6,6)-phenyl-C_{61}-butyric acid.

visible regions. For example, the response rise time is around 0.3 s while the decay time is around 1.0 s when the illumination is 500 nm (Fig. S21). Cyclic switching on/off upon incident light illumination demonstrates that the device exhibits highly reproducible photodetecting behavior and photo-stability at visible light (Fig. 4b and Fig. S20).

Upon illumination of the optimized incident light (500 nm) and bias voltage (5.0 V), the device shows a high detectivity (D^*) of 4.88×10^{12} Jones, and an exceptionally large external quantum efficiency (EQE) of 2866% (Fig. 4c), which is consistent with its high R_λ value (11.6 A W^{-1}, Fig. 4a). Under the above-mentioned measurement conditions, D^* and EQE are positively correlated with R_λ. These results demonstrate that the 2D polymeric cuprofullerene material exhibits excellent photodetective performance [3–5]. The photocurrent was enhanced with increaseing illumination (Fig. 4d). A simple power law model, $I_p \propto P^\theta$, was used to describe the relationship between photocurrent I_p and incident light power P. The exponent, θ, was fitted at 0.77 ($0.5 < \theta < 1$), implying significant defects in the crystalline structure and complicated photocurrent processes (Fig. S22) [3,5].

In summary, an ultra-stable 2D cuprofullerene imidazolate coordination polymer was prepared under solvothermal conditions. Linear μ_2-η^2:η^2-C_{60} molecules connected 1D Cu(I)-imidazolate chains to form a 2D sheet structure. Intersheet convex-concave π···π interactions further supported the ability of these C_{60} moieties to form a highly ordered *i-hfp* feature and increase its chemical and thermal stability. Band structure calculations and photodetector device measurements revealed that its high photodetective performance was inherited not only from *fcc* and *hcp* crystalline structures of pristine C_{60}, but also significantly enhanced and improved by the complexation of Cu(I). This research provides an effective strategy for preparing exohedral metallofullerene polymers, thereby producing high-performance photodetective functions in the cuprofullerene polymers, leading to advantageous opportunities for expanding exohedral metallofullerene polymers as novel fullerene-based photoelectric materials.

Received 5 September 2020; accepted 11 December 2020; published online 15 January 2021

1 Kroto HW, Heath JR, O'Brien SC, *et al.* C_{60}: Buckminsterfullerene. Nature, 1985, 318: 162–163
2 Gong X, Tong M, Xia Y, *et al.* High-detectivity polymer photodetectors with spectral response from 300 nm to 1450 nm. Science, 2009, 325: 1665–1667
3 Saran R, Curry RJ. Solution processable 1D fullerene C_{60} crystals for visible spectrum photodetectors. Small, 2018, 14: 1703624
4 Zheng S, Xiong X, Zheng Z, *et al.* Solution-grown large-area C_{60} single-crystal arrays as organic photodetectors. Carbon, 2018, 126: 299–304
5 Liu K, Gao S, Zheng Z, *et al.* Spatially confined growth of fullerene to super-long crystalline fibers in supramolecular gels for high-performance photodetector. Adv Mater, 2019, 31: 1808254
6 Yang D, Zhou X, Ma D. Fast response organic photodetectors with high detectivity based on rubrene and C_{60}. Org Electron, 2013, 14: 3019–3023
7 Kang H, Lee W, Oh J, *et al.* From fullerene–polymer to all-polymer solar cells: the importance of molecular packing, orientation, and morphology control. Acc Chem Res, 2016, 49: 2424–2434
8 Wu KY, Wu TY, Chang ST, *et al.* A facile PDMS-assisted crystallization for the crystal-engineering of C_{60} single-crystal organic field-effect transistors. Adv Mater, 2015, 27: 4371–4376
9 Wang J, Xu L, Zhang B, *et al.* n-Type doping induced by electron transport layer in organic photovoltaic devices. Adv Electron Mater, 2017, 3: 1600458
10 Balch AL, Winkler K. Two-component polymeric materials of fullerenes and the transition metal complexes: a bridge between metal–organic frameworks and conducting polymers. Chem Rev, 2016, 116: 3812–3882
11 Liu X, Kozlowska M, Okkali T, *et al.* Photoconductivity in metal–organic framework (MOF) thin films. Angew Chem Int Ed, 2019, 58: 9590–9595
12 Goswami S, Ray D, Otake KI, *et al.* A porous, electrically conductive hexa-zirconium(iv) metal–organic framework. Chem Sci, 2018, 9: 4477–4482

 © Science China Press and Springer-Verlag GmbH Germany, part of Springer Nature 2021

13 Yang F, Cheng S, Zhang X, *et al.* 2D organic materials for optoelectronic applications. Adv Mater, 2018, 30: 1702415
14 Huang Q, Zhuang G, Jia H, *et al.* Photoconductive curved-nanographene/fullerene supramolecular heterojunctions. Angew Chem Int Ed, 2019, 58: 6244–6249
15 Liu YM, Xia D, Li BW, *et al.* Functional sulfur-doped buckybowls and their concave-convex supramolecular assembly with fullerenes. Angew Chem Int Ed, 2016, 55: 13047–13051
16 Li B, Zhen J, Wan Y, *et al.* Anchoring fullerene onto perovskite film *via* grafting pyridine toward enhanced electron transport in high-efficiency solar cells. ACS Appl Mater Interfaces, 2018, 10: 32471–32482
17 Hwang IW, Xu QH, Soci C, *et al.* Ultrafast spectroscopic study of photoinduced electron transfer in an oligo(thienylenevinylene): fullerene composite. Adv Funct Mater, 2007, 17: 563–568
18 Sariciftci NS, Smilowitz L, Heeger AJ, *et al.* Photoinduced electron transfer from a conducting polymer to buckminsterfullerene. Science, 1992, 258: 1474–1476
19 Wang C, Wang H, Liu C, *et al.* Molecular assembly-induced charge transfer between a mixed (phthalocyaninato)(porphyrinato) yttrium triple-decker and a fullerene. Inorg Chem Front, 2019, 6: 654–658
20 Jiang X, Yuan M, Liu H, *et al.* Optoelectronic properties of one-dimensional fullerene nanorods. Mater Lett, 2016, 176: 52–55
21 Saran R, Stolojan V, Curry RJ. Ultrahigh performance C_{60} nanorod large area flexible photoconductor devices *via* ultralow organic and inorganic photodoping. Sci Rep, 2014, 4: 5041
22 Geng J, Zhou W, Skelton P, *et al.* Crystal structure and growth mechanism of unusually long fullerene (C_{60}) nanowires. J Am Chem Soc, 2008, 130: 2527–2534
23 Zhan SZ, Zhang GH, Li JH, *et al.* Exohedral cuprofullerene: sequentially expanding metal olefin up to a C_{60}@Cu_{24} rhombicuboctahedron. J Am Chem Soc, 2020, 142: 5943–5947
24 Chu D, Liu Y, Li Y, *et al.* Journey to the holy grail of a coordination saturated buckyball. Inorg Chem Front, 2020, 7: 2556–2559
25 Lebedeva MA, Chamberlain TW, Khlobystov AN. Harnessing the synergistic and complementary properties of fullerene and transition-metal compounds for nanomaterial applications. Chem Rev, 2015, 115: 11301–11351
26 Konarev DV, Khasanov SS, Nakano Y, *et al.* Linear coordination fullerene C_{60} polymer $[\{Ni(Me_3P)_2\}(\mu\text{-}\eta^2, \eta^2\text{-}C_{60})]_\infty$ bridged by zerovalent nickel atoms. Inorg Chem, 2014, 53: 11960–11965
27 Aghabali A, Jun S, Olmstead MM, *et al.* Silver(I)-mediated modification, dimerization, and polymerization of an open-cage fullerene. J Am Chem Soc, 2016, 138: 16459–16465
28 Peng P, Li FF, Bowles FL, *et al.* High yield synthesis of a new fullerene linker and its use in the formation of a linear coordination polymer by silver complexation. Chem Commun, 2013, 49: 3209–3211
29 Chancellor CJ, Olmstead MM, Balch AL. Formation of crystalline polymers from the reaction of amine-functionalized C_{60} with silver salts. Inorg Chem, 2009, 48: 1339–1345
30 Lee K, Song H, Park JT. [60]Fullerene−metal cluster complexes: Novel bonding modes and electronic communication. Acc Chem Res, 2003, 36: 78–86
31 Grądzka E, Wysocka-Żołopa M, Winkler K. *In situ* conductance studies of two-component C_{60}-Pd polymer. J Phys Chem C, 2014, 118: 14061–14072
32 Nagashima H, Nakaoka A, Saito Y, *et al.* $C_{60}Pd_n$: the first organometallic polymer of buckminsterfullerene. J Chem Soc Chem Commun, 1992, 377
33 Tanaka M, Yamanaka S. Vapor-phase growth and structural characterization of single crystals of magnesium doped two-dimensional fullerene polymer Mg_2C_{60}. Cryst Growth Des, 2018, 18: 3877–3882
34 Zhan SZ, Li JH, Zhang GH, *et al.* Coordination disk-type nano-Saturn complexes. Chem Commun, 2020, 56: 3325–3328
35 Huang XC, Zhang JP, Chen XM. A new route to supramolecular isomers *via* molecular templating: nanosized molecular polygons of copper(I) 2-methylimidazolates. J Am Chem Soc, 2004, 126: 13218–13219
36 Santiso-Quiñones G, Reisinger A, Slattery J, *et al.* Homoleptic Cu–phosphorus and Cu–ethene complexes. Chem Commun, 2007, 53: 5046
37 Jayaratna NB, Cowan MG, Parasar D, *et al.* Low heat of adsorption of ethylene achieved by major solid-state structural rearrangement of a discrete copper(I) complex. Angew Chem Int Ed, 2018, 57: 16442–16446
38 Seo DK, Hoffmann R. Direct and indirect band gap types in one-dimensional conjugated or stacked organic materials. Theor Chem Acc, 1999, 102: 23–32
39 Liu J, Zhou W, Liu J, *et al.* Photoinduced charge-carrier generation in epitaxial mof thin films: High efficiency as a result of an indirect electronic band gap? Angew Chem Int Ed, 2015, 54: 7441–7445
40 Alers GB, Golding B, Kortan AR, *et al.* Existence of an orientational electric dipolar response in C_{60} single crystals. Science, 1991, 257: 511–514
41 Wen C, Li J, Kitazawa K, *et al.* Electrical conductivity of a pure C_{60} single crystal. Appl Phys Lett, 1992, 61: 2162–2163
42 Mort J, Ziolo R, Machonkin M, *et al.* Electrical conductivity studies of undoped solid films of $C_{60/70}$. Chem Phys Lett, 1991, 186: 284–286

Acknowledgements This work was financially supported by the National Natural Science Foundation of China (21731002, 21975104, 22071141 and 21471094), Guangdong Major Project of Basic and Applied Research (2019B030302009), and Guangdong Basic and Applied Basic Research Foundation (2019A1515012162).

Author contributions Zhan SZ contributed to data analysis and wrote the paper with support from Li Y. Li JH performed the synthesis and characterizations. Li Y and Xu G fabricated the photodetector device, measured and discussed the photoelectronic performance. Luo DF and Dang L performed the band structure calculations. Li D supervised the project. All authors contributed to the general discussion.

Conflict of interest The authors declare that they have no conflict of interest.

Supplementary information Crystallographic data (CCDC no. 2000096), Experimental and characterization details, physical measurements, theoretical calculations and photoelectric effects are available in the online version of the paper.

© Science China Press and Springer-Verlag GmbH Germany, part of Springer Nature 2021

Shun-Ze Zhan obtained his BSc degree (1999) from China Three Gorges University, and PhD degree (2012) from Shantou University supervised by Professor Dan Li. He is currently an associate professor at Shantou University. His research interest is the design and fabrication of photofunctional coinage metal complexes and exohedral metallofullerene materials.

Dan Li obtained his BSc (1984) and PhD (1993) degrees from Sun Yat-Sen University and The University of Hong Kong, respectively. He worked in Shantou University and moved to Jinan University in 2016. His research interest is the design and fabrication of supramolecular coordination assemblies and their functions.

具有高性能可见光探测功能的超稳定二维咪唑铜(I)富勒烯配位聚合物材料

詹顺泽[1*], 李经鸿[1], 李艳周[3,4], 徐刚[3], 骆登峰[1], 党丽[1], 李丹[2*]

摘要 本工作通过溶剂热法制备了一种超稳定二维层状铜(I)富勒烯配位聚合物材料. Cu-(η^2-C_{60})配位作用和层间凹凸π···π相互作用支撑C_{60}分子排列形成倾斜六方面堆积((*i-hfp*))特点, 显著地改善了材料的化学稳定性. 该材料表现出高性能可见光探测功能. 密度泛函计算表明, 与六方紧密堆积和立方堆积的C_{60}纳米材料类似, 其优异的光探测功能主要来源于C_{60}分子本身, 但是铜(I)的配位显著增强了其对可见光的吸收效率, 改善了材料的可见光探测功能. 该工作对于拓展富勒烯光电功能材料的种类具有重要意义.

 © Science China Press and Springer-Verlag GmbH Germany, part of Springer Nature 2021